Human Molecular Genetics, 2019, Vol. 28, No. 10 1709–1725

doi: 10.1093/hmg/ddz016
Advance Access Publication Date: 24 January 2019
General Article

GENERAL ARTICLE

Deleting nebulin's C-terminus reveals its importance to sarcomeric structure and function and is sufficient to invoke nemaline myopathy

Frank Li[1,†], Elisabeth R. Barton[2] and Henk Granzier[1,*]

[1]Department of Cellular and Molecular Medicine, University of Arizona, Tucson, Arizona, 85721, USA and
[2]Department of Applied Physiology and Kinesiology, University of Florida, Gainesville, Florida, 32611, USA

*To whom correspondence should be addressed at: Medical Research Building, RM 325, 1656 E Mabel St, Tucson, AZ 85721. Tel: (520) 6689339; Email: granzier@email.arizona.edu

Abstract

Nebulin is a large skeletal muscle protein wound around the thin filaments, with its C-terminus embedded within the Z-disk and its N-terminus extending out toward the thin filament pointed end. While nebulin's C-terminus has been implicated in both sarcomeric structure and function as well as the development of nemaline myopathy, the contributions of this region remain largely unknown. Additionally, the C-terminus is reported to contribute to muscle hypertrophy via the IGF-1 growth pathway. To study the functions of nebulin's C-terminus, we generated a mouse model deleting the final two unique C-terminal domains, the serine-rich region (SRR) and the SH3 domain ($Neb^{\Delta 163–165}$). Homozygous $Neb^{\Delta 163–165}$ mice that survive past the neonatal stage exhibit a mild weight deficit. Characterization of these mice revealed that the truncation caused a moderate myopathy phenotype reminiscent of nemaline myopathy despite the majority of nebulin being localized properly in the thin filaments. This phenotype included muscle weight loss, changes in sarcomere structure, as well as a decrease in force production. Glutathione S-transferase (GST) pull-down experiments found novel binding partners with the SRR, several of which are associated with myopathies. While the C-terminus does not appear to be a limiting step in muscle growth, the IGF-1 growth pathway remained functional despite the deleted domains being proposed to be essential for IGF-1 mediated hypertrophy. The $Neb^{\Delta 163–165}$ mouse model emphasizes that nebulin's C-terminus is necessary for proper sarcomeric development and shows that its loss is sufficient to induce myopathy.

Introduction

Nebulin is a long filamentous protein that contributes to the structure of the skeletal muscle sarcomere. Its size ranges from 600 to 900 kDa and it exists wound around the actin thin filaments (1). It is comprised primarily of repeated modules with its C-terminus embedded within the Z-disk and its N-terminus extending out toward the ends of the thin filaments (2). Nebulin's ability to bind to the thin filament arises from the actin-binding sequences present in each of the repeated modules that make up 97% of the protein (3). Most of those modules are further organized into seven-module, homologous super-repeats, with mice containing 25 super-repeats (SR1–SR25). Each super-repeat has an additional tropomyosin binding site that allows for the further integration of nebulin into the thin filaments (4). Due to its size and localization within the sarcomere, nebulin was initially believed to interact with proteins along the length of the thin filament and be the primary contributor to thin filament length regulation (5). While recent findings have instead suggested it supports the formation of the thin filament but does not quite encompass the entirety of some thin

[†]Frank Li, http://orcid.org/0000-0002-2969-6713
Received: June 26, 2018. **Revised:** December 17, 2018. **Accepted:** January 10, 2019

filaments (6), nebulin's role as a major thin filament regulator remains. The remaining non-actin-binding domains of nebulin exist as a glutamic acid-rich region at the N-terminus and two domains at the C-terminus: a serine-rich region (SRR) and an SH3 domain (3).

Initial *in vivo* studies involving nebulin's function in the sarcomere were done primarily with nebulin knockout mouse models (7,8). Following this, it was reported that in addition to thin filament length regulation nebulin also contributes to cross-bridge cycling and force generation as well as Z-disk alignment and width regulation (9–11). As studies moved toward understanding growth and regeneration, a novel myofibrillar hypertrophy mechanism involving nebulin's C-terminus was also proposed (12). This mechanism involves the actin-polymerization protein N-WASP being sequestered to the Z-disks during IGF-1 stimulation, allowing for interaction between N-WASP and nebulin and resulting in myofibrillogenesis. What makes this mechanism stand out is the role of the two C-terminal domains, with the SRR being a target of phosphorylation and the SH3 domain activating N-WASP. These different studies emphasize that nebulin is a multifunctional protein that is vital to several sarcomeric functions. With these advances in knowledge, it became necessary to study the protein piece by piece in order to understand how different domains contribute to the overall function of nebulin.

The two non-actin-binding C-terminal domains in nebulin, the SRR and the SH3 domain, were studied because of their location in the Z-disk, predicted important functions and potential role in nemaline myopathy. The SH3 domain was initially predicted to anchor nebulin to the Z-disks and many studies on this domain proposed additional interactions with other structural proteins (3,7,12–15). However, it was also recently found to be dispensable to nebulin function, suggesting those previously reported interactions were not essential for disease formation or protein function *in situ* (16). Comparatively little is known about the SRR due to lack of studies, but based on observations in patient studies, myopathy phenotypes may be caused by the loss of both domains (17).

The hypothesis that these domains contribute to myopathy stems from the observation that their loss appears to contribute to nemaline myopathy, with 55% of patients having some form of truncating mutation that would all result in the loss of these unique domains (18,19). Additionally, there was no correlation between the amount of protein truncated and the severity of the disease, with patients having lost as little as the C-terminal domains plus a few actin-binding modules manifesting a severe myopathy (17,20,21). In all these patients, nebulin's C-terminus exists as a point of similarity that suggests that, to better characterize the myopathy phenotype, an in-depth understanding of nebulin's C-terminus is required. In order to successfully study the structural and functional effects of losing both C-terminal domains, a mouse model expressing a truncated nebulin lacking specifically nebulin's two C-terminal domains was created. Following the characterization of the mouse model, unique interactions with the less understood SRR as well as the model's ability to undergo muscle hypertrophy were also studied.

Results

Characterization of the Neb$^{\Delta 163-165}$ model

To investigate the role of nebulin's unique C-terminal domains in the skeletal muscle sarcomere, a mouse model that would produce a nebulin protein lacking the SRR and the SH3 domain was generated. In order to remove those domains from the endogenous *Neb* locus, homologous recombination was performed using a vector containing a series of stop codons followed by an FRT-flanked neomycin cassette. The location of these stop codons after the start of murine exon 163 allowed for the complete translation of the final actin-binding module, M206 (Fig. 1B). Flp recombination was used to remove the neomycin cassette and the integration of the stop codons was verified via PCR analysis (Fig. 1C). Within the first week, it was visibly apparent that there was a weight deficit in the homozygous mice. This deficit carried through into adulthood and mice remained significantly lighter than their wild-type counterparts even at 1 year of age (Fig. 1D). However, the truncation of nebulin also had a severe impact on the postnatal survivability of the homozygous mice, resulting in 10% of the total population being homozygous when genotyped ~10 days after birth (Fig 1F). This skewed Mendelian ratio is likely due to deaths soon after birth as the distribution of embryonic genotypes was normal and few deaths were ever observed past the 1 week time point (Fig. 1G; Supplementary Material, Fig. S1A). Despite the initial high mortality rate, 87% of surviving homozygous mice survived to adulthood (Fig. 1E). Interestingly, the observed weight loss at multiple time points was not due to an inherently smaller mouse since tibia lengths, an indicator of growth that can influence muscle weight (22), was not significantly altered (Supplementary Material, Fig. S1B). In summary, we created a mouse model lacking the two C-terminal nebulin domains in which homozygous mice live to adulthood and the *in vivo* functions of the SRR and SH3 domain can be studied.

Changes in skeletal muscle weight and myosin heavy chain distribution

Analysis of distal limb muscles revealed that several had decreased weights compared to wild type, especially in the gastrocnemius, plantaris and quadriceps where weights were reduced by ~50% (Fig. 2A and B). These deficits persisted through adulthood and despite a slight lag in homozygous muscle weight at 6 months, limb muscle weights remained at a constant ratio to wild-type weights, returning to the same ratio by 12 months (Fig. 2C). In performing gel electrophoresis on multiple limb muscles, every muscle studied was found to have a significant shift in their myosin heavy chain (MHC) composition (Fig. 3A and B). The shift trended toward slower fiber types, resulting in a reduced ratio of IIB (fast) fibers and increased IIA/X (middling) and I (slow) fibers. Even muscles that did not originally have a prominent type I fiber population, such as the extensor digitorum longus (EDL), gained a small population of those fibers (Table 1).

Importantly, muscles that did not display a weight reduction, such as the soleus and the EDL, both experienced this compositional shift. To better understand these changes in the absence of an overt weight deficit, the changes occurring in individual fiber types that likely accompanied this shift were investigated. Specifically, the EDL was studied due to the appearance of the type I fibers, which are not typically expressed in this muscle. Here it was found that there was a significant increase in the number of fibers in the homozygous EDL, with both IIX and IIB fibers experiencing significant increases in fiber count (Fig. 3C). However, despite having more fibers, IIB fibers account for a smaller fraction of the whole cross-sectional area (CSA), while the area covered by IIX fibers increases (Fig. 3D). Slower fiber types such as type I and IIA experience a significant increase in fiber size but neither appears to contribute significantly to the maintenance of the EDL weight (Fig. 3E and F). Conversely, faster

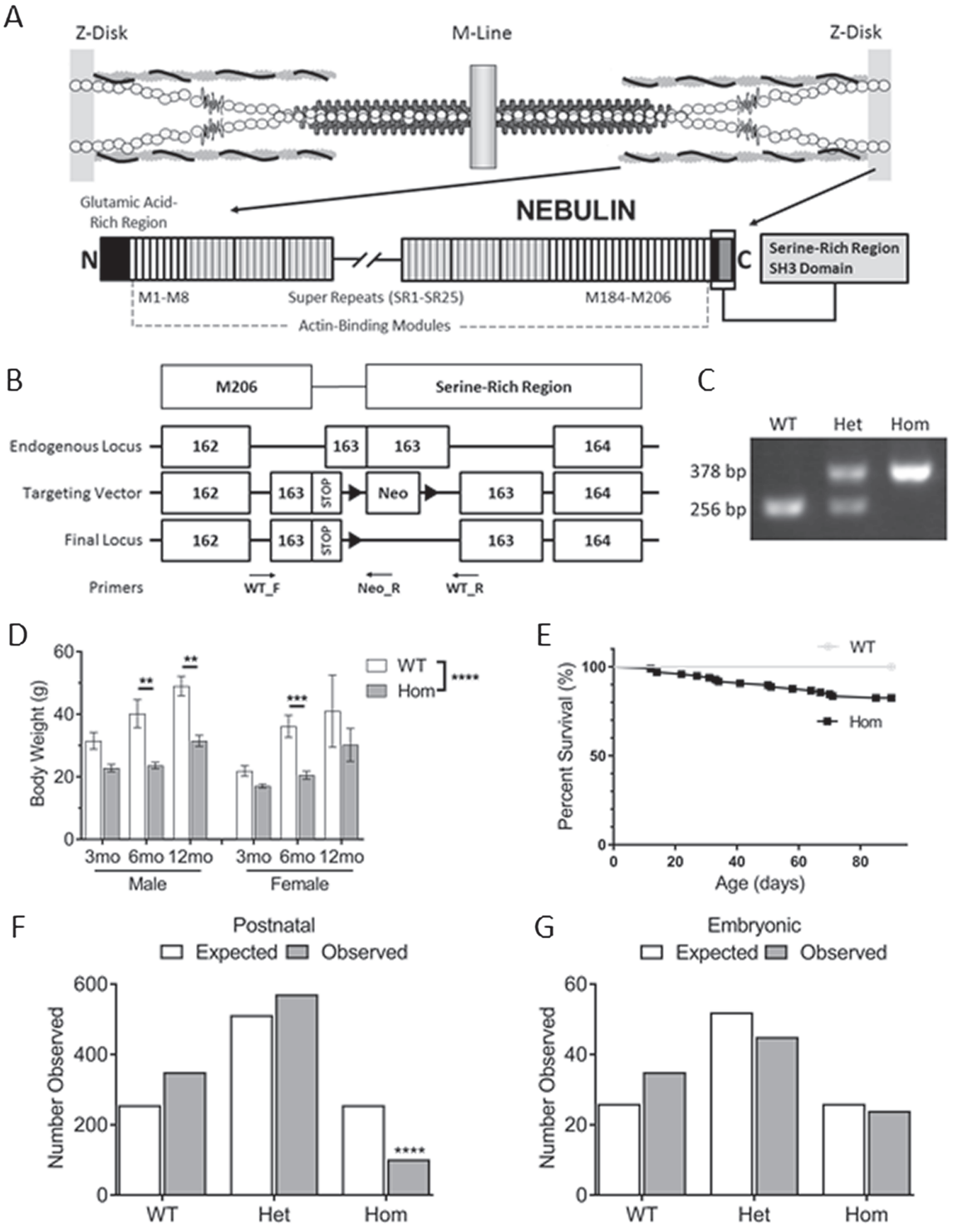

Figure 1. Neb$^{\Delta 163–165}$ model development and postnatal phenotype. (**A**) Location of nebulin in the sarcomere. The final two domains at the C-terminus are emphasized. (**B**) Generation of the truncation model. Location of the final actin-binding module, M206 is indicated. Black triangles are FRT sites. Removal of the C-terminal domains was accomplished via stop codons within Exon 163 followed by neo cassette removal via Flp recombination. Locations of forward and reverse primers used to identify truncation indicated. (**C**) PCR confirmation of nebulin truncation following neomycin cassette removal. Difference in size is indicative of remaining FRT site and linkers used in the recombination. (**D**) Mouse weight comparison at three different time points (male: $n = 5, 5, 4$; female: $n = 12, 8, 5$). Homozygous mice remain lighter through adulthood. (**E**) Postnatal survival ($n = 97$). Postnatal deaths were observed as early as 1 week of age. (**F** and **G**) Distribution of genotypes in embryonic and postnatal mice from Het × Het breeding pairs (postnatal, $n = 1023$; embryonic, $n = 101$). Postnatal genotypes significantly different from Mendelian ratios.

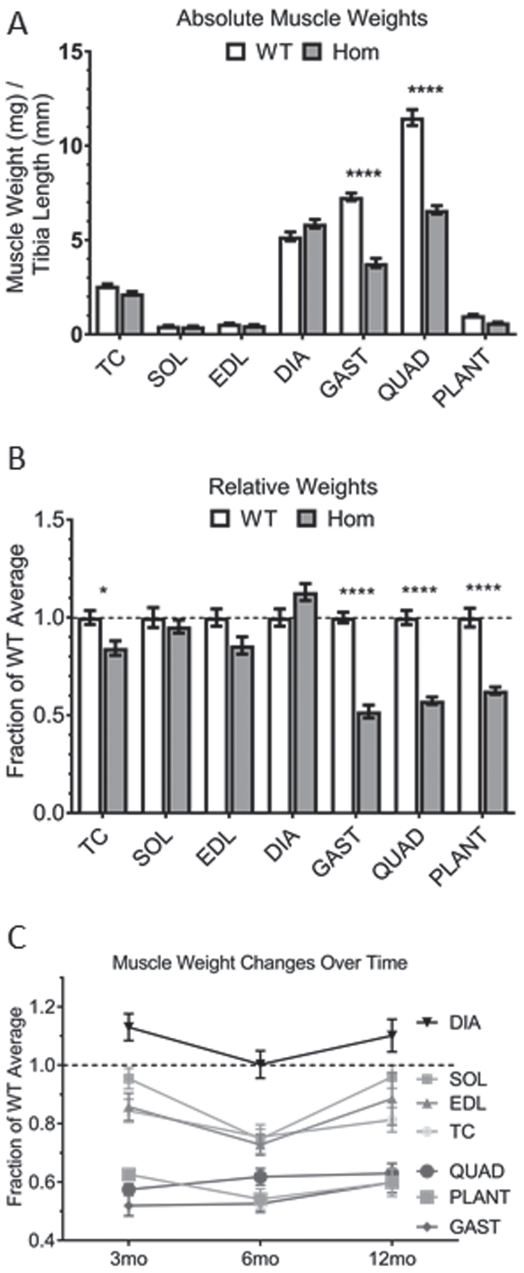

Figure 2. Muscle weight analysis. (**A** and **B**) Muscle weights at 3 months ($n = 9$–10). Raw values are normalized to tibia length. Relative weights obtained by normalization to wild-type averages. (**C**) Muscle weight deficits observed throughout homozygous lifespan ($n = 9, 6, 4$). Two-way ANOVA reveals age has a significant effect on the diaphragm ($P < 0.0001$), with soleus trending ($P = 0.06$) and EDL being not significant ($P = 0.3$).

fiber types become significantly smaller (Fig. 3G and H). These data show that it is a combination of hyperplasia of the IIB and IIX fibers as well as retention of type IIX fiber size that results in the homozygous EDL matching the wild-type EDL in overall weight.

Variations in nebulin protein expression and the retention of thin filament length regulation

To determine how well the truncated nebulin was being transcribed and translated, western blots were performed on different limb muscles using antibodies to the N- and C-terminus of nebulin. It was found in the homozygous mice that while the N-terminus was intact, as expected, the SRR and SH3 domains were missing (Fig. 4A). Those results further confirmed the proper truncation of the protein. Quantification of N-terminal expression revealed that several muscles had reduced nebulin protein expression (Fig. 4B). This protein deficit in homozygous tissues was observed at multiple time points, but that deficit did not significantly change throughout those time points. Surprisingly, the homozygous soleus maintained wild-type levels of nebulin protein expression. Quantification of the mRNA transcript using qRT-PCR showed that in fact there was a persistent deficit of nebulin transcript in all limb muscles, including the soleus (Fig. 4C). This indicates that the truncation of nebulin's C-terminus is affecting the stability of the mRNA transcript and may be playing a role in the decreased nebulin protein expression.

Despite the truncation, nebulin was still able to insert into the Z-disk. Domains near the truncation were localized in the Z-disk using an antibody to modules M197 through M202 [originally referred to as M176-M181 (23)], with the final actin-binding module (M206) being only four domains away (Fig. 5A and B). Additionally, nebulin was still able to localize properly to the thin filaments, with the N-terminus forming an expected doublet near the H-zone of the sarcomeres (Fig. 5C). The specificities of both the N-terminal antibody and the M176-M181 antibody were demonstrated in nebulin exon 55 knockout tissues, which are completely deficient in nebulin (24) (Supplementary Material, Fig. S2A,B). These data show that nebulin still aligns with the thin filaments. This was further supported by the observation that thin filament lengths in both the soleus and the EDL were not significantly different between wild-type and homozygous mice (Fig. 5D). These findings indicate that while the loss of the C-terminus may affect protein stability during translation, nebulin has nevertheless retained its ability to regulate the thin filament lengths.

Effects on sarcomere structure and Z-disk width regulation

To test the hypothesis that loss of the C-terminus is sufficient to induce the mild myopathic phenotype observed, namely the weight deficits and fiber-type switching, limb muscle structure and function was studied. The soleus and the EDL, two functionally opposing muscles, were used with the soleus representing a slow-twitch muscle and the EDL representing a fast-twitch muscle. The sarcomeres of both muscle types were analyzed using electron microscopy. Protein aggregates were found in both muscles, with the EDL exhibiting a more severe phenotype [Fig. 6A, comparing top (WT) to bottom (Hom)]. These aggregates, commonly referred to as nemaline rod bodies (25), were largely found in line with the Z-disks and disrupt the organization of the sarcomeres (Fig. 6A, arrows). These observations show that on average, the soleus contained larger rod bodies than the EDL, but those occurred with lower frequency, resulting in less total sarcomeric area being occupied by protein aggregates (Fig. 6B and C).

It was also noted in the homozygous muscles that Z-disk widths from aggregate-lacking sarcomeres appeared different, especially in the EDL (Fig. 6D and E). When multiple fibers in these two muscles were analyzed, the soleus exhibited a small but significant decrease in Z-disk widths while the EDL exhibited a large increase (Fig. 6F and G). These data could both be explained by a combination of the MHC composition changes

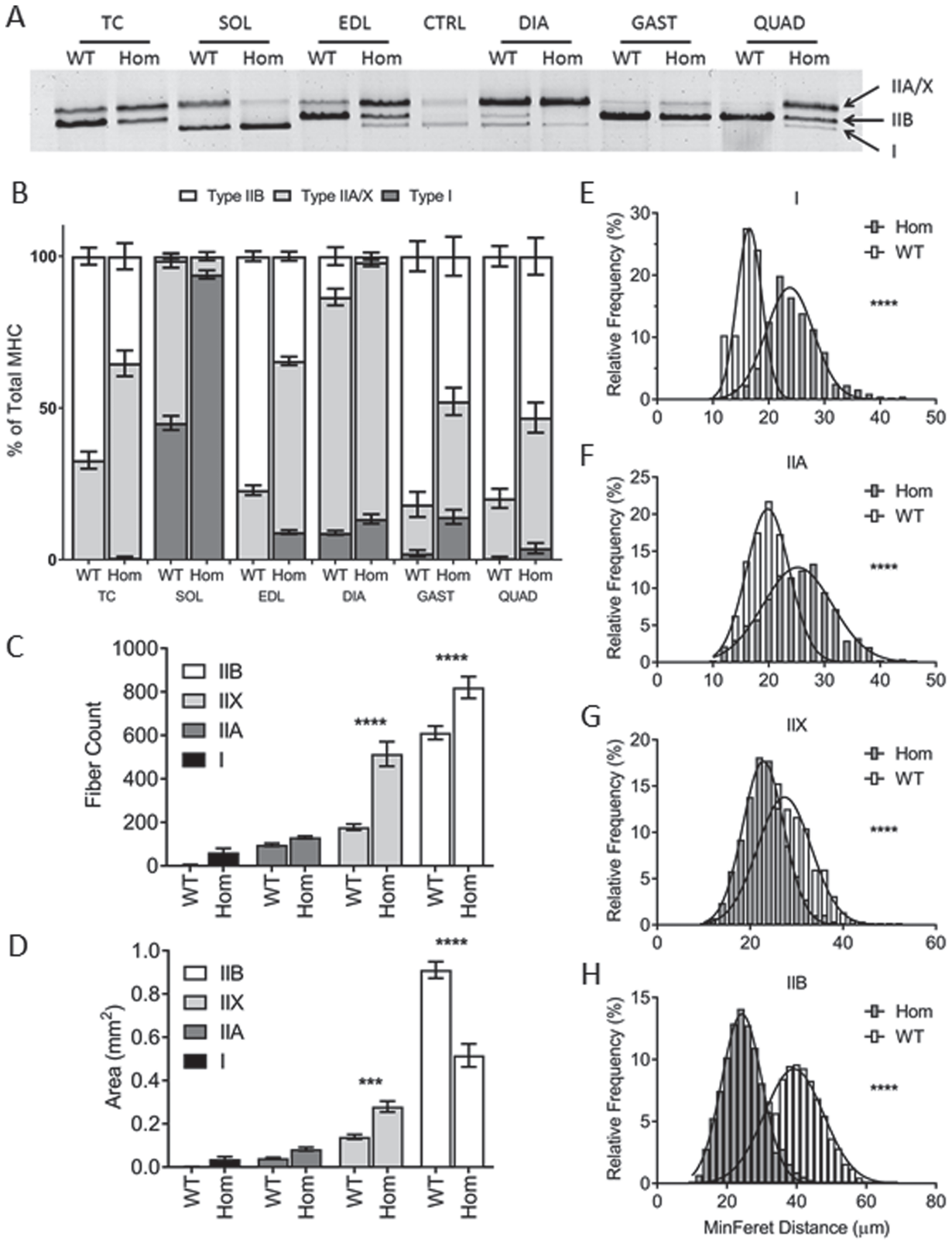

Figure 3. Myosin heavy chain changes and EDL composition. (**A**) Representative acrylamide gel of MHC fiber type ratios in both wild-type and homozygous mice. Control sample is a mix of TC and SOL from C57BL/6 J mouse. (**B**) Graphical representation of changes in ratios between wild-type and homozygous mice ($n = 12$). Shift to slower fiber types indicated by increasing fractions of both type IIA/X and type I. Statistics of changes presented in Table 1. (**C**) Distribution of different fiber types in the EDL muscle ($n = 9, 7$). IIB and IIX fibers are significantly greater ($P < 0.0001$) in the homozygous tissue. (**D**) Area covered by different fiber types in the EDL muscle ($n = 9,7$). IIB area is significantly reduced ($P < 0.0001$) while IIX area is significantly increased ($P < 0.001$). (**E–H**) Changes in minimum Feret diameter of fiber types in the EDL muscle. In slower fiber types (I and IIA), homozygous fibers were on average significantly larger ($P < 0.0001$) while in faster fiber types (IIX and IIB), homozygous fibers were on average significantly smaller ($P < 0.0001$).

Table 1. Two-Way ANOVA analysis of MHC expression for each muscle comparing WT and HOM fibers

Fiber type	IIB, *P*-value	IA/X, *P*-value	I, *P*-value
TC	<0.0001	<0.0001	NS
SOL	NS	<0.0001	<0.0001
EDL	<0.0001	<0.0001	<0.0001
DIA	<0.001	<0.05	NS
GAST	<0.0001	<0.01	NS
QUAD	<0.0001	<0.001	NS

TC, tibialis cranialis; SOL, soleus; EDL, extensor digitorum longus; DIA, diaphragm; GAST, Gastrocnemius; QUAD, quadriceps.

observed and the loss of nebulin's C-terminus. While wider Z-disks are associated with slower fiber types (26), the loss of nebulin's C-terminus may also influence the width of the Z-disks to a small degree, leading to the changes seen in the soleus. However, because the EDL is a fast-twitch muscle and has much thinner Z-disks compared to the soleus, the shift to slower fiber types is dominant as reflected in the drastic widening of its Z-disks.

Effects on muscle contractility

In quantifying the contractility of both EDL and soleus using force-frequency protocols on isolated muscle, it was found that while the EDL displayed a drastic loss of force, the force loss in the soleus was much more subtle (Fig. 7A and B). Using two-way analysis of variance (ANOVA) while taking into account force production over multiple time points, the homozygous soleus did in fact have a significant force loss (Fig. 7C and D). Additionally, while the homozygous EDL muscle could contract and relax in the same amount of time as the wild-type muscle, deficits were noted in the soleus, specifically in the time it took for the muscle to complete a single twitch and the time it took to relax after tetanus (Supplementary Material, Fig. S3A–D). Considering the normal weight and nebulin protein expression of the soleus, these data show that the loss of nebulin's C-terminus is responsible for the slight changes in contractility observed in this muscle.

Earlier work by Yamamoto *et al.* showed that the removal of nebulin's SH3 domain resulted in increased sensitivity to eccentric contraction (EC) damage but did not cause other phenotypes (16). The same stimulation-and-stretch EC injury protocol was performed on the largest head of the EDL muscle, known as the fifth-toe EDL, and experiments found a similar trend toward lower forces post-EC damage (Fig. 7E). However, due to the inherent force deficit in whole EDL, detailed above, only a trending association toward increased EC damage was observed (Supplementary Material, Fig. S3E). More prominently, the homozygous EDL had a higher rate of force loss during the EC injury protocol (Fig. 3F). Overall, these results support the findings that loss of the SH3 domain results in an increased sensitivity to EC-induced injury and shows that the loss of the SRR in addition to the SH3 domain leads to large force deficits.

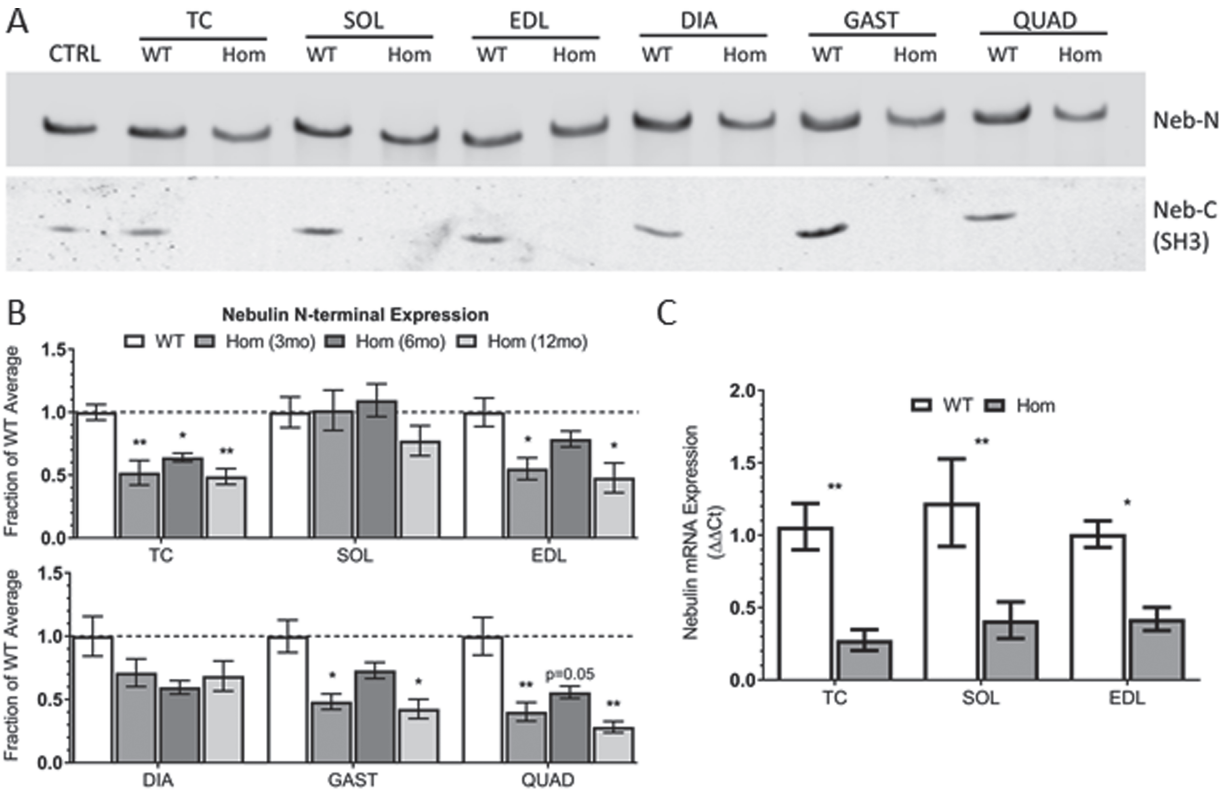

Figure 4. Effects of truncation on nebulin protein and mRNA expression. (**A**) Representative western blot utilizing several hind limb muscles. Truncation confirmed through SH3 antibody due to complete absence of signal. (**B**) Quantification of nebulin protein expression through N-terminal antibody signal and normalized to MHC content over multiple time points ($n = 8, 8, 6$). Soleus protein expression is comparable to wild type. Two-way ANOVA shows age has no effect on protein expression in homozygous soleus. (**C**) Quantification of mRNA expression in TC, soleus and EDL. Homozygous tissues have significantly less mRNA expression in all muscles tested: TC ($P < 0.01$), SOL ($P < 0.01$) and EDL ($P < 0.05$).

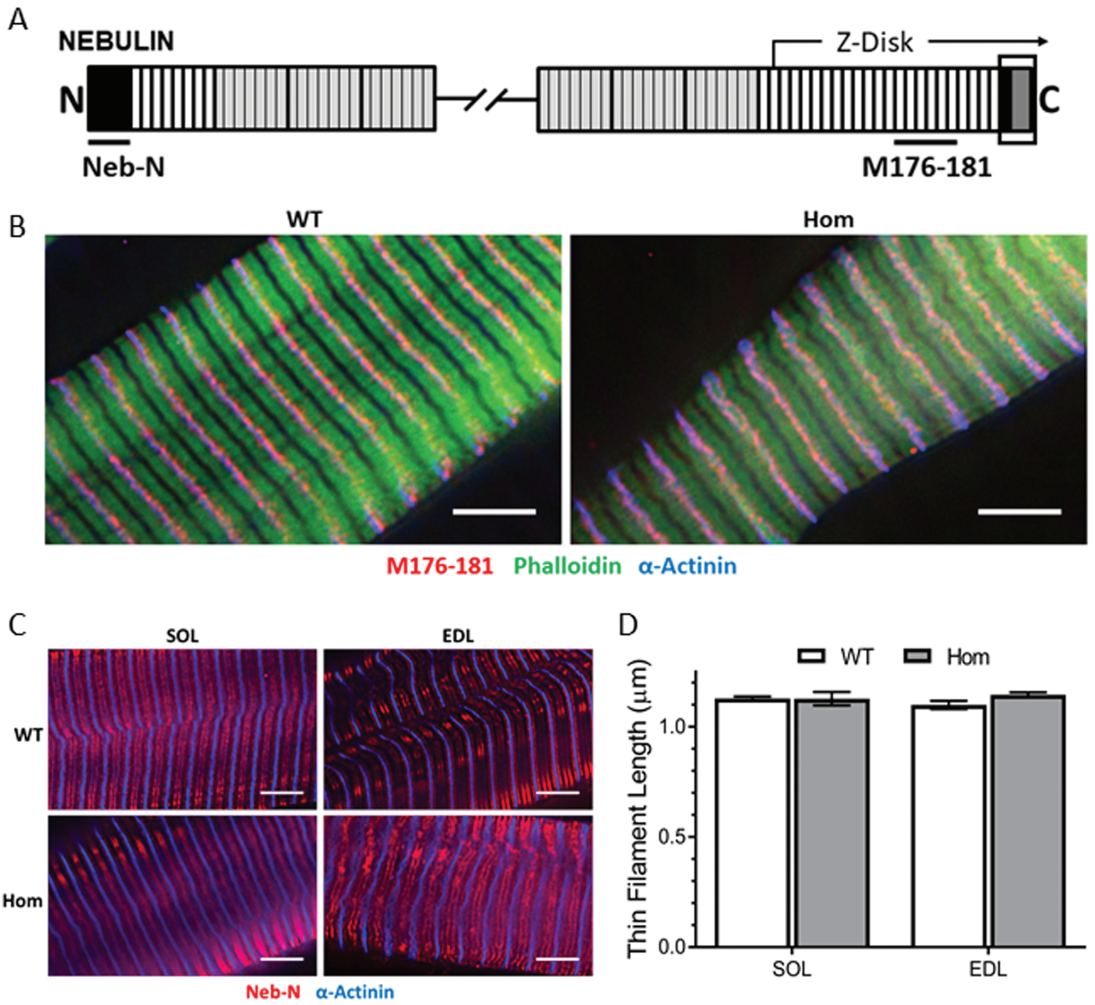

Figure 5. Protein localization and thin filament length regulation. (**A**) Diagram of antibody locations. The section of nebulin embedded within the Z-disk is identified. (**B**) Localization of modules M197-M202 (α-M176-M181, red) in EDL along with phalloidin (green) and α-actinin (blue). Modules colocalize with α-actinin at the Z-disks (scale bar: 5 μm). (**C**) Localization of nebulin in the sarcomere utilizing the nebulin N-terminal antibody (red) and an α-actinin antibody (blue) to identify the Z-disks. Doublet near the H-zone of the sarcomere was identified as nebulin (scale bar: 5 μm). (**D**) Thin filament length comparison in soleus and EDL. Soleus is not significantly different, EDL trends to slightly longer thin filaments ($P = 0.06$; $n = 4, 6, 9, 7$).

Discovery of novel binding partners of the SRR

Glutathione S-transferase (GST) pull-down experiments were run with whole-muscle lysate using single-domain GST-bound constructs of the SRR and the SH3 domain as well as a two-domain construct that mirrored the endogenous C-terminus. The two-domain construct also allowed for the verification of single-domain interactions because true physiological interactions found in single-domain constructs should also interact with the two-domain construct. From two independent pulldowns of these constructs, a band appearing ~65 kDa was prominent and occurred in both SRR-containing constructs (i.e. alone or in combination with SH3) but not when using the SH3 domain only (Fig. 8A). Within this band, mass spectrometry results consistently reported proteins associated with both skeletal muscle and general metabolism (Table 2). Additionally, three of these proteins have been previously reported to lead to other myopathies when disrupted: myotilin, KLHL41 and AIFM1. These proteins were chosen for further study based on their reported contributions to the sarcomeres and reported associations with myopathies.

Myotilin, a prominent regulator of Z-disk width (32), was significantly overexpressed in several of the limb muscles studied (Fig. 8C). Kelch-like protein 41, or KLHL41, a nemaline myopathy-associated gene (28), did not show significant increases in specific limb muscles, though through two-way ANOVA, there is an overall increase in KLHL41 protein expression (Fig. 8D). Finally, apoptosis-inducing factor, mitochondrial 1 (AIFM1) was found to mimic myotilin expression, with significantly higher expression found in the tibialis cranialis (TC), EDL, gastrocnemius and quadriceps (Fig. 8E). Considering this protein's role in apoptosis (29), changes in this protein may also contribute to the myopathy phenotype observed. Localization of all three proteins was investigated and no significant changes were found (Supplementary Material, Fig. S4).

IGF-1-mediated hypertrophy mechanism

Based on a novel hypertrophy model (12), it is expected that the loss of nebulin's C-terminal domains attenuates the hypertrophy

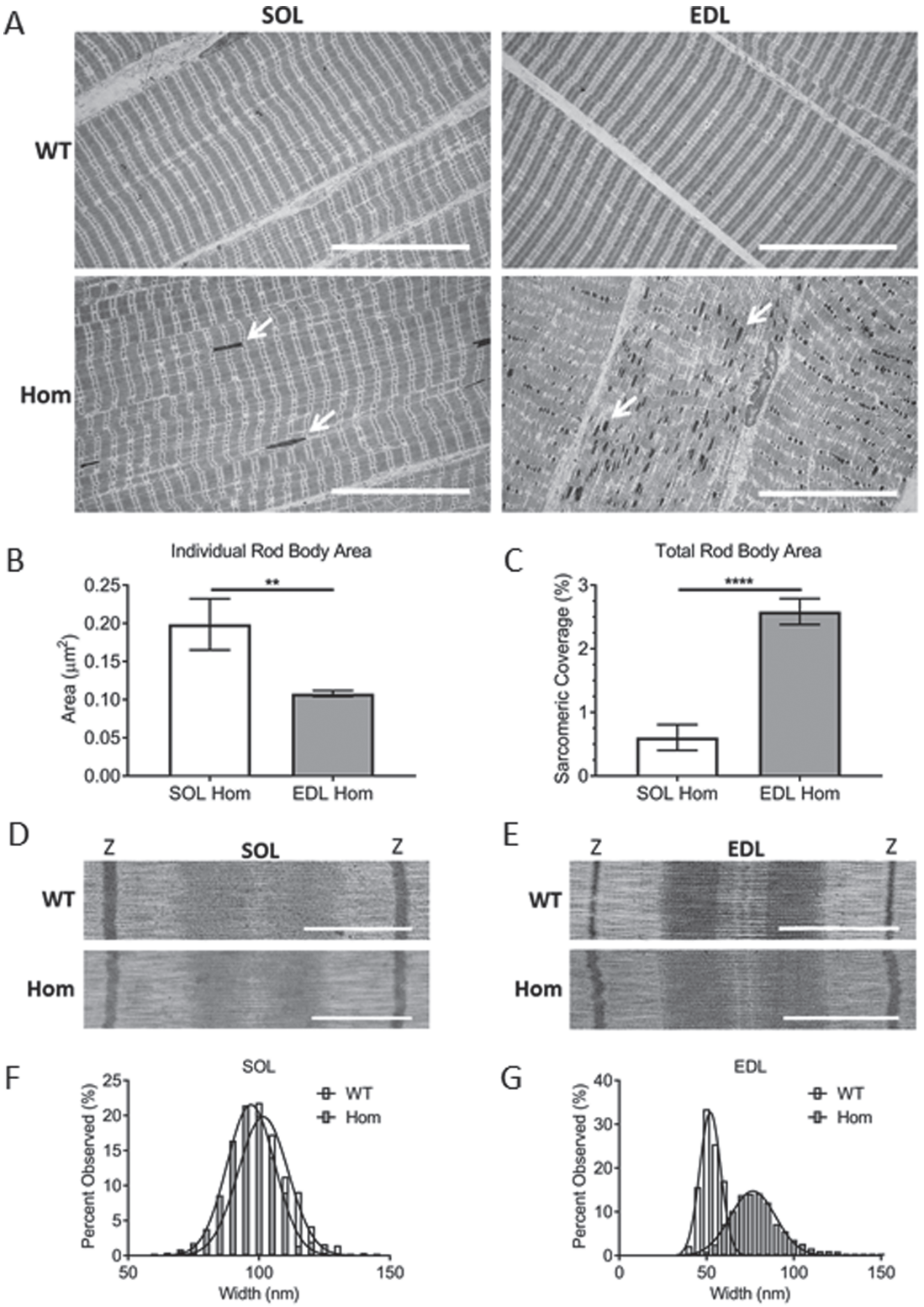

Figure 6. Structural studies on the sarcomeres. (**A**) Low magnification view of fiber bundles (scale bar: 25 μm). Protein aggregates (white arrows) observed frequently in EDL, infrequently in soleus. (**B**) Quantification of the size of rod bodies observed and (**C**) percent area covered by rod bodies in sampled images. Data were gathered as follows: soleus, 102 images across 20 unique fibers; EDL, 135 images across 29 unique fibers (from $n = 2$ mice). While EDL contains smaller protein aggregates, they appear more frequently and cover significantly more area in muscle fibers compared to the soleus. (**D** and **E**) Examples of sarcomeres without Z-disk aggregates in homozygous mice of soleus and EDL compared to wild type (scale bar: 1 μm). Homozygous EDL Z-disks have a distinct widening compared to wild type. (**F** and **G**) Quantification of non-aggregate Z-disk widths in soleus and EDL ($n = 11$–29 unique fibers). Approximately five measurements were made from five unique images taken per fiber (WT SOL, 550; HOM SOL, 500; WT EDL, 275; HOM EDL, 666 measurements). Soleus exhibits a slight but significant decrease in widths while EDL exhibits a drastic increase in widths.

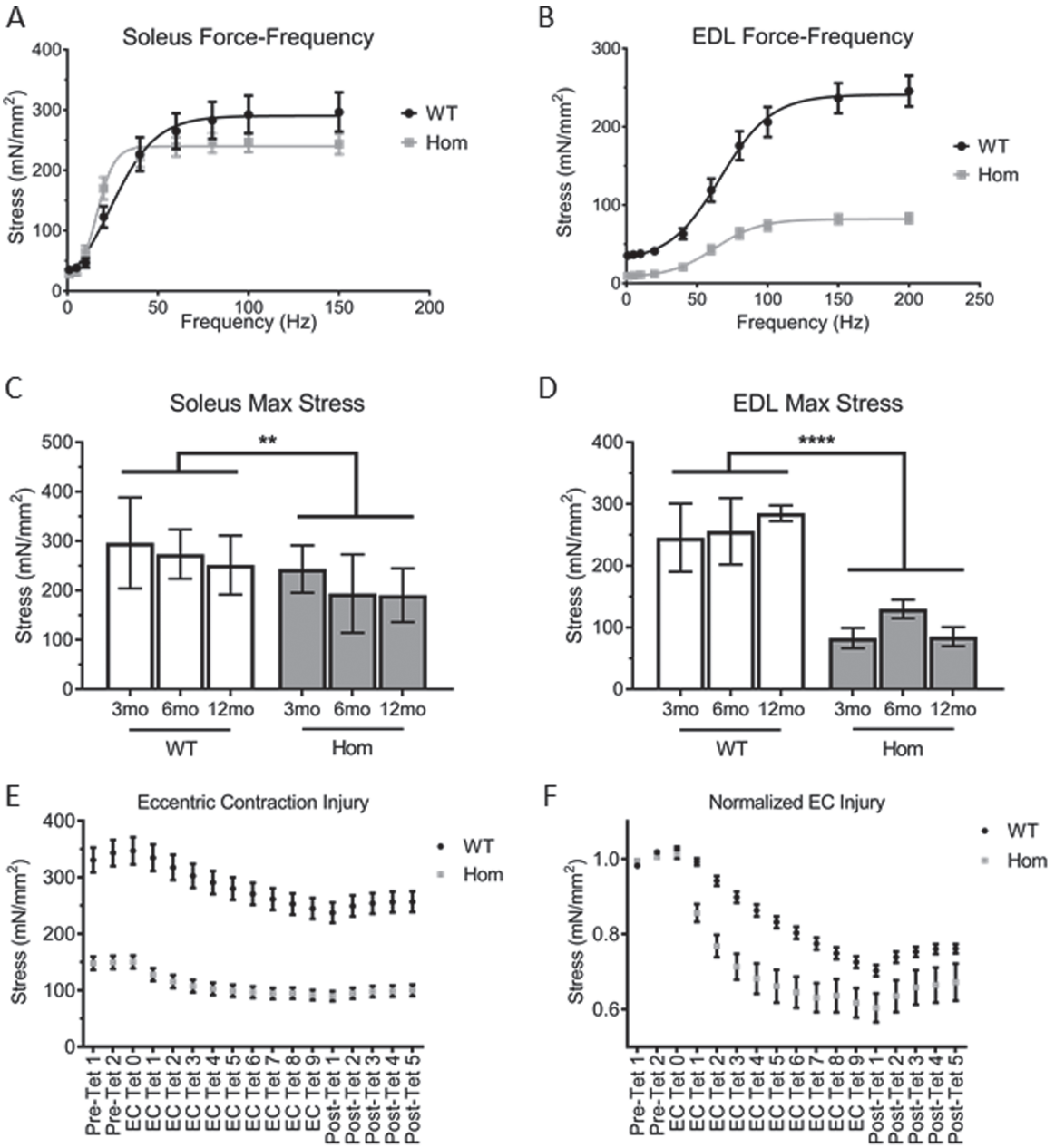

Figure 7. Functional studies using whole muscle mechanics. (**A** and **B**) Force–frequency relationship of the soleus and EDL at 3 months. Slight reduction of half-max frequency in the soleus not observed at any other time point or in the EDL. (**C** and **D**) Max stress produced by the soleus and EDL at various time points (soleus, $n = 8, 6, 7$; EDL, $n = 7,4,6$). Two-way ANOVA indicates that the slight decrease in soleus is significant. (**E**) EC injury protocol ($n = 10$). Similar to homozygous whole EDL, the fifth-toe EDL muscle exhibits a significant force drop in baseline tetanus. (**F**) Normalized EC injury protocol. All forces normalized to average pre-injury force. Homozygous tissue loses force exponentially faster than wild type during the injury protocol.

response to IGF-1 stimulus. In short, this is because nebulin's SRR is proposed to be phosphorylated by GSK-3β, preventing the interaction between the SH3 domain and the branched actin-forming protein, N-WASP. Through IGF-1 stimulation GSK-3β is inhibited, allowing for this interaction to occur and leading to myofibrillar hypertrophy. To test this mechanism, TC muscles were subjected to an intramuscular injection of an IGF-1 AAV and the effect was quantified for both the TC and the neighboring EDL after 1 month. One-way ANOVA showed that IGF-1 increased TC and EDL weights in wild-type mice by ∼15% (Fig. 9A–C). However, the homozygous muscles responded in a similar manner and a similar ∼15% increase in weights was observed. The endogenous expression of IGF-1 in treated TCs was verified via ELISA to ensure both wild-type and homozygous tissues had been successfully treated (Supplementary Material, Fig. S5). A quantification of the individual fibers from the AAV-treated EDL found no significant differences between the wild-type and homozygous hypertrophy response in each fiber type (Fig. 9D).

Discussion

After nebulin was established as a major contributor of nemaline myopathy, studies turned toward therapies that focused on

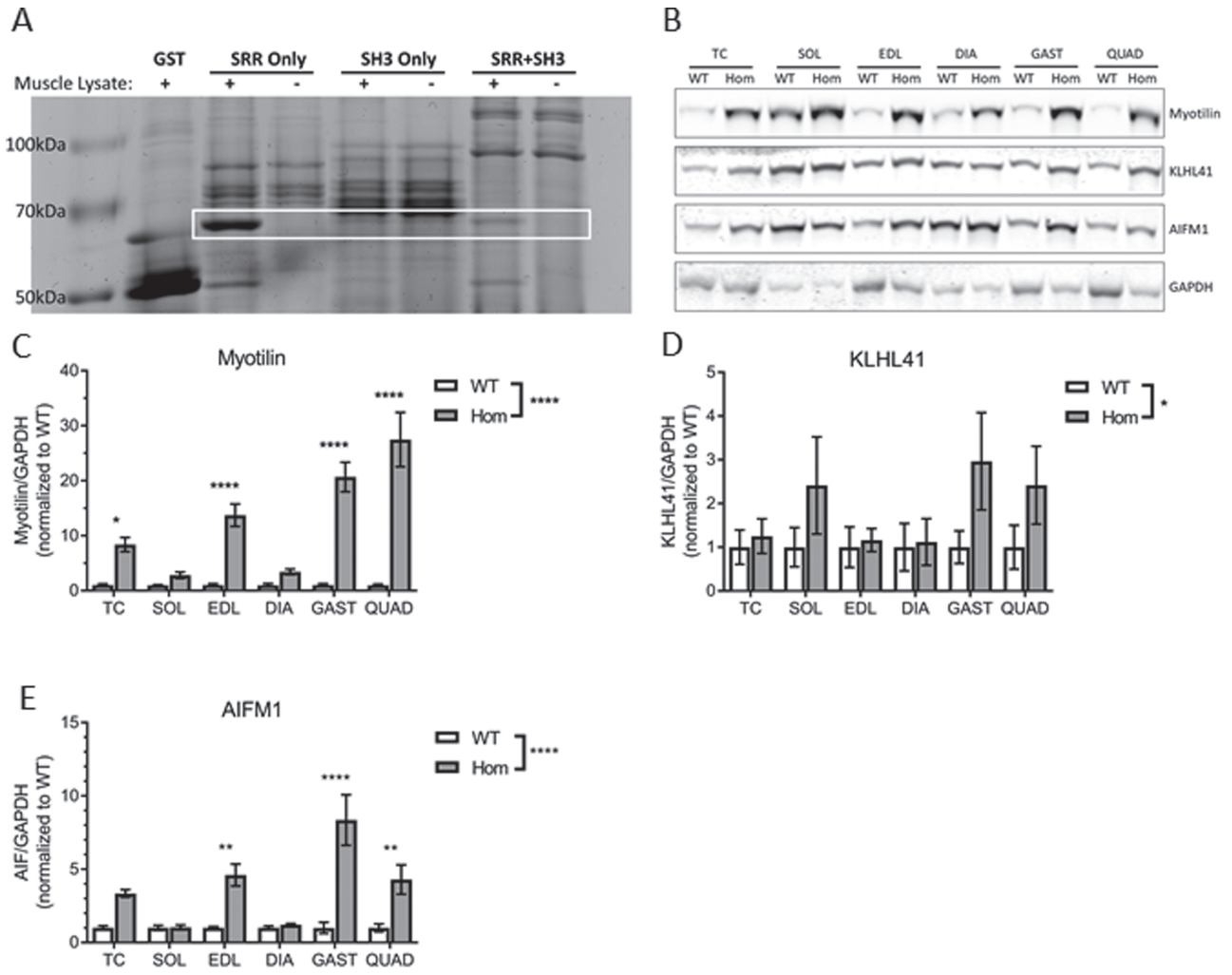

Figure 8. GST pulldown with whole muscle lysate. (**A**) Section of an 8% acrylamide gel revealing the most prominent band located within the pulldown using a GST-tagged SRR at ~65 kDa. This band is also found in the GST construct containing both the SRR and the SH3 domain. (**B**) Western blot examples for myopathy-related proteins found in pulldown. (**C**) Protein expression of myotilin ($n = 6$). TC, EDL, gastrocnemius and quadriceps all significantly increased. Two-way ANOVA also shows significant increases in protein expression in homozygous mice compared to wild type. (**D**) Protein expression of KLHL41 ($n = 6$). A global increase in homozygous tissue protein expression compared to wild type is observed. (**E**) Protein expression of AIFM1 ($n = 6$). EDL, gastrocnemius and quadriceps have significant increases. TC has a trending increase ($P = 0.07$). Two-way ANOVA also shows significant increases in protein expression in homozygous mice compared to wild type.

increasing the force of contraction (33,34). However, this meant that understanding of the protein was limited to findings based on the full knockout of a multifunctional protein. The only domain-specific study utilizing a nebulin truncation revealed a minimal function of the SH3 domain (limiting EC damage) (16) but nothing that related to nebulin's more established functions of thin filament length regulation, force production or structural regulation of the Z-disks (7–11). It was however proposed that the SRR acted as a signaling hub or that the two domains together had a greater function in the sarcomere (16). This study examined a novel nebulin model that exhibits a more severe myopathy phenotype, compared to the SH3 knockout model, through the removal of only two C-terminal domains, the SRR and the SH3 domain. Through this truncation, the experiments show that these C-terminal domains play a significant role in developing the structural and functional integrity of the sarcomere and are sufficient to invoke a nemaline myopathy phenotype.

Viability of the truncation model

$Neb^{\Delta 163–165}$ mice are born at Mendelian ratios, but many homozygous mice die shortly after birth. The mice that survive exhibit a weight deficit within the first week and 87% of those remaining live into adulthood with no further complications. Surviving homozygous mice appear healthy and do not have any outward abnormalities other than a slight weight difference. Additionally, the discovery of stillborn mice only hours after birth suggests an early postnatal deficit (Supplementary Material, Fig. S1A). A lack of milk spots in all pups of those groups indicate that it was more likely a respiratory problem despite no drastic weight differences being observed in the diaphragm later in life (Fig. 2C). A possible explanation is that even slight deficits in nebulin protein expression in the diaphragm can result in contractile issues after birth, something that has been observed in infant patients (20,25). If this is the case, then some homozygous mice overcome this hurdle, but approximately half do not, leading to a

Table 2. Recurrent proteins identified from separate spectroscopy analyses

Recurring proteins	Associated myopathy	Unique peptides
Myotilin	**Myofibrillar myopathy** (27)	**7**
KLHL41	**Nemaline myopathy** (28)	**5**
AIFM1	**Encephalomyopathy** (29)	**5**
ACADVL	Myopathy in late-onset VLCAD deficiency (30)	14
ATAD3	None (mitochondrial activity), loss in muscles leads to myopathy phenotype (31)	9
ARFGAP2	None (protein metabolism)	6
HNRNPK	None (mRNA metabolism and transport)	3

non-Mendelian ratio when quantified at 10 days after birth. This emphasizes the role of nebulin's C-terminus in postnatal muscle development as the original conventional nebulin knockout model also exhibited severe muscle weakness at birth quickly followed by death within approximately the first week (7,8).

Mice expressing a truncated nebulin may be able to live longer than their conventional knockout counterparts due to their ability to produce and retain nebulin, albeit at a reduced level in some muscles. However, there does not appear to be a correlation between muscle atrophy and nebulin protein expression. For instance, while muscles like the soleus and the EDL had weights comparable to the wild-type controls, the amount of nebulin each muscle contained was unaltered in the soleus but reduced by ~40% in the EDL. Furthermore, despite varying levels of nebulin protein expression over time, the rate of muscle growth remained comparable between wild-type and homozygous mice, resulting in a consistent ratio between homozygous and wild-type weight at multiple time points (Fig. 2C). This suggests that there is no direct correlation between nebulin protein expression and muscle growth. Rather, nebulin is likely to be more vital to the initial postnatal development of the sarcomeres, contributing little to muscle growth later in life. The lack of worsening phenotypes also implies that structural contributions of nebulin are more important during early development. This new model shows that while the C-terminal domains of nebulin contribute to postnatal survivability, the mice surviving this initial event display a much milder myopathy phenotype than full knockout models.

Changes in MHC fiber content and compensatory effects

The truncation of nebulin resulted in all distal limb muscles experiencing a compositional shift toward slower fiber types (Fig. 3B). Changes in fiber type composition of sedentary mice suggest changes in the metabolic requirements and can imply a pathological origin (35). This set of experiments showed that despite some limb muscles appearing to be unaffected by the truncation of nebulin there was an underlying myopathy that affected all skeletal muscles.

As observed in the EDL the changes in MHC composition were not necessarily due to a loss of fast fiber types, but rather hyperplasia alongside a reduction in their CSAs. Here the EDL, which experiences a drastic shift in fiber composition, undergoes hyperplasia to maintain weight comparable to the wild-type muscle. The most likely scenario is that truncation of

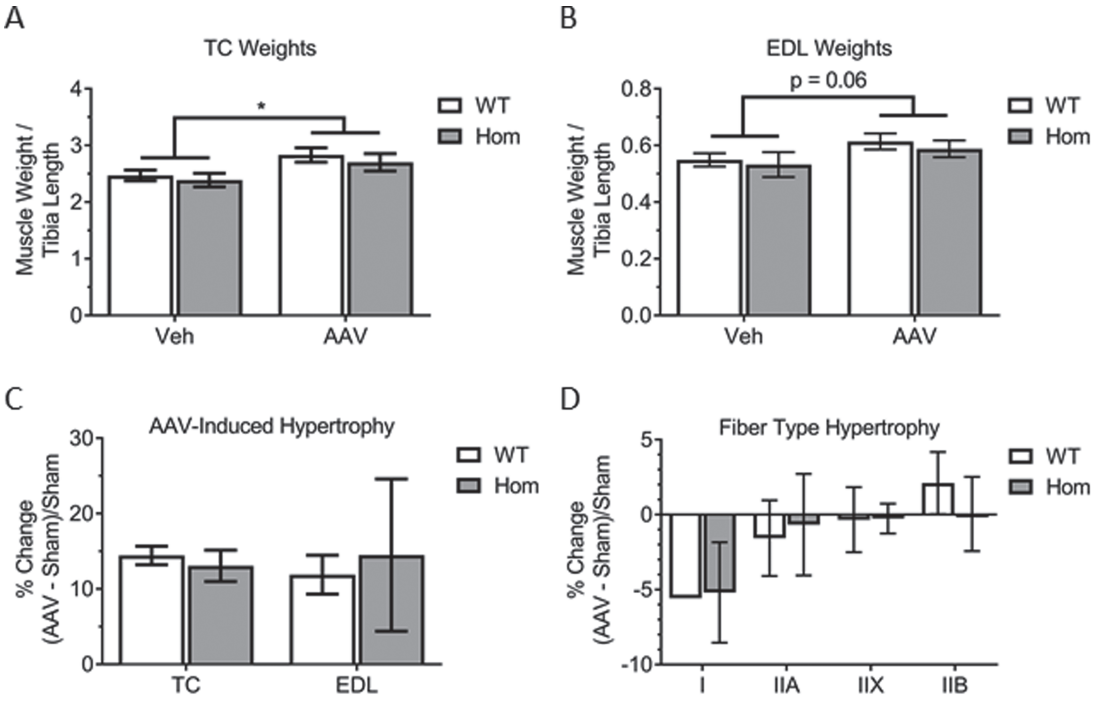

Figure 9. Injection of IGF-1 AAV to induce muscle hypertrophy. **(A)** Changes observed between treated and untreated legs for both TC and EDL ($n = 10, 7$). Intramuscular injections performed on TC and AAV diffuses to the EDL. Injected TCs are significantly heavier than the PBS-injected TCs. Diffused EDLs trend to higher weights as well. **(C)** Percent change of the leg injected with the AAV compared to the PBS-injected leg. No significant differences found in muscle weight change. **(D)** Fiber-type specific width analysis performed using MinFeret values. Percent change between AAV-injected and sham-injected legs reported, no significant differences found in fiber hypertrophy.

nebulin results in muscle weakness, which in turn causes changes in protein regulation and mitochondrial biosynthesis to order to increase the size of slower fiber types (36). Conversely, fast fibers do not tolerate changes in nebulin as well, a phenomenon documented in the conditional knockout model (11). Apparently, some additional growth pathway is influencing the hyperplasia of fast fibers to maintain muscle mass and allowing the muscle to generate more force than it would have in the complete absence of nebulin. One proposed mechanism of myofibrillogenesis, specifically involving IGF-1 stimulation, is detailed later on in this discussion.

Loss of the C-terminus and specific nebulin functions

In full nebulin knockout models, studies found an overall shortening of the thin filaments with an increased variation in thin filament lengths (7,8,11). Filaments were found to be as short as 0.4 μm and few fibers were able to reach the expected 1.0–1.2 μm range (7). Comparatively, such a loss in the organization of the thin filaments was not observed in the $Neb^{\Delta 163–165}$ model. Nebulin was clearly able to localize properly to the thin filaments and the lengths observed through phalloidin staining indicated there was no difference between wild-type and homozygous mice. There were slight density changes in the A-band in the EDL when observed using electron microscopy wherein the H-zone was not well defined in homozygous EDL. This was attributed to a characteristic commonly seen in tissues with more prominent slow fiber types, namely the soleus and the heart, and seems to reflect the dramatic shift toward slower fiber types in the homozygous EDL. Overall, these findings indicate that nebulin's C-terminus is not playing a major role in thin filament length regulation.

An effect that was found is force loss, a common symptom observed in nemaline myopathy (25). The loss of nebulin's C-terminus appears partially responsible for the severe force loss observed in previously studied full knockout models. As observed in these experiments, both the soleus and the EDL experienced force loss at multiple time points though the loss was less apparent in the soleus (Fig. 7C and D). And compared to previous studies, this loss was not as severe (7,8,11). When considering that a reduction in nebulin protein expression may contribute to additional force loss, the soleus shows that even if a truncated nebulin is expressed to wild-type levels, there will still be a force deficit.

The effects of the C-terminal truncation are additionally observed through the alterations in the Z-disk width, where the EDL experiences a drastic increase while the soleus exhibits a slight decrease in width. The implication from the soleus is that nebulin's C-terminus plays a minor role in Z-disk width regulation. With the soleus becoming almost completely type I fibers, an increase in Z-disk width is expected (26). The decrease in width compared to the wild-type distribution suggests that loss of the C-terminus is preventing the soleus Z-disk from reaching the expected larger width.

The observation of protein aggregates in line with the Z-disks suggests that protein turnover is also partially compromised within the Z-disk, resulting in the formation of nemaline rod bodies through a small truncation of nebulin. The truncation appears to be destabilizing the Z-disk structure, which would impair any contributions it may have to overall force production (26). These findings suggest that nebulin's C-terminus has a partial contribution to force generation, possibly through its interaction with other proteins that maintain the stability of the Z-disk.

SRR and myopathy phenotypes

While the SRR has been proposed to facilitate C-terminal localization of nebulin to the Z-disks (37), it has not been studied in animal model systems. Conversely, the SH3 domain has been much more prominently featured in functional studies (7,12–15). When the SH3 domain deletion model did not reveal any myopathy phenotypes or changes in previously predicted protein interactions, the SRR became the target of our studies. A standard GST pulldown with three different combinations of the two domains as bait was performed to elucidate this domain. Considering the results from single-domain and two-domain constructs, a prominent band observed at ~65 kDa represented interactions with the removed domains. Interestingly, this band was not replicated in the SH3 domain pulldown suggesting that the interactions were specific to the SRR alone. The proteins identified within this prominent band were found to be associated with metabolism, protein turnover and structure, with three of the seven recurring proteins being contributors to various myopathies. These findings suggest that the SRR of nebulin plays an important role in the regulation of sarcomere structure and its loss may be a primary contributor to the development of myopathy.

Myotilin is a prominent regulator for the formation of the Z-disks, interacting with α-actinin and filamin-C to help stabilize the Z-disk (38). Mutations within this protein are also known to lead to myopathy (32). AIFM1 on the other hand is a pro-apoptotic protein that additionally helps maintain mitochondrial bioenergetics (39). Both myotilin and AIFM1 were differentially upregulated in the skeletal muscle studied. Specifically, both proteins appeared to be more upregulated in muscles that normally have more fast fibers. For myotilin, this may be related to changes observed at the Z-disk, particularly in the EDL (Fig. 6E and G), with widening Z-disks and protein aggregates a result of its upregulation. These findings also coincide with reports that overexpression of myotilin can worsen a myopathy phenotype, wherein mice had a more rapid onset of myofibrillar aggregation and more severe muscular degeneration (40). AIFM1 is more associated with the bioenergetics of cells (39) and its upregulation appears to correlate instead with the changes in fiber composition (Fig. 3B). That both proteins are more upregulated in fast muscles indicates muscle type-specific alterations. One possibility is that the SRR is a signaling hub that helps regulate both the Z-disk widths and sarcomere bioenergetics. An increase in tension cost (11) results in an attempt to produce more ATP, resulting in AIFM1 being upregulated. Simultaneously, myotilin becomes overexpressed as the fibers take on traits of slower fiber types, leading to both widening Z-disks and an increase of protein aggregate presence (Fig. 6A, bottom right). To investigate the possibility of bioenergetics playing a role in the phenotypes observed, ACADVL, identified in the pulldown, was also tested. Western blot showed a significant increase in protein expression in fast-twitch fibers, similar to that seen in AIFM1 and myotilin (Supplementary Material, Fig. S6). Further investigation of these protein interaction may help explain why faster muscle types exhibit more severe myopathy phenotypes than slower muscle types (11).

KLHL41, on the other hand, can lead to nemaline myopathy when mutated (28). Recently, its ability to stabilize nebulin and prevent myopathy was also elucidated (41). In the $Neb^{\Delta 163–165}$ model, KLHL41 was not significantly upregulated in any one muscle, though two-way ANOVA indicated that the genotype was having a significant effect on KLHL41 protein expression.

This slight upregulation may indicate that KLHL41 does not rely wholly on the SRR for its function. Also, the previous characterization of KLHL41 utilized its interaction with nebulin's super-repeats (41), suggesting that that this protein interacts with multiple regions of nebulin. A more in depth study on the interaction between KLHL41 and the SRR needs to be performed to clarify how it impacts the published function in nebulin stabilization (41).

To verify these interactions, a reverse pulldown was performed using a purified SRR construct lacking the GST tag (Supplementary Material, Fig. S7). Recombinant KLHL41, myotilin and AIFM1 were produced with a GST tag on the N-terminus of these proteins using the same method as the nebulin C-terminal constructs. This experiment showed no binding between recombinant protein and purified SRR, suggesting several possibilities. One possibility is that expression in a bacterial cell may not be ideal for these proteins. There may be significant differences in processes such as folding or post-translational modification between the host cell used and skeletal muscle, which may affect the binding affinity. Another possibility is that these proteins were initially pulled down by the GST-tagged SRR through an indirect interaction, whereby the accessory proteins would be missing in this experiment. More stringent experiments are required to fully establish the interactions between the SRR and these three proteins.

Hypertrophy and nebulin

Based on the study of nebulin's contribution to myofibrillar hypertrophy, nebulin's SH3 domain interacts with the branched actin-forming protein N-WASP while the SRR acting as a phosphorylation site regulating this interaction (12). The Neb$^{\Delta 163–165}$ model makes it possible to critically test this proposed mechanism through the removal of those two key domains. An IGF-1 AAV was used to create a chronic overexpression of the signaling protein. This would elucidate the differences in muscle hypertrophy caused by these missing domains. However, chronic elevation of IGF-1 failed to reveal a difference between wild-type and homozygous mice. The injected TC in both genotypes underwent the same amount of hypertrophy and the neighboring EDL followed that same trend. Studies on individual fiber types also failed to reveal any significant differences in the hypertrophic response. This finding is supported by the published SH3 deletion model, where they also failed to reproduce the nebulin-N-WASP interaction following acute IGF-1 stimulation (16). Thus, nebulin's C-terminus is not a limiting factor for the proposed IGF-1 hypertrophy mechanism. This does, however, imply that nemaline myopathy patients exhibiting C-terminal truncations may still benefit from therapeutics utilizing the IGF-1 pathway. Further experiments should be done to determine why a non-linear actin forming protein like N-WASP would be localizing to the Z-disks and if there is a C-terminal independent mechanism influencing the formation of new actin filaments.

Conclusions

Nebulin's C-terminus plays a crucial role in early postnatal development of muscles. Loss of C-terminal domains induces a fast-to-slow compositional shift in muscle fibers, which in turn results in changes in Z-disk structure. This two-domain truncation affects force output, resulting in reduced forces at all time points tested. However, once those early developmental changes are set, the mouse continues to develop and the myopathy phenotypes do not worsen. The cause for these changes may in part be attributed to the lost interactions with the signaling region that is the SRR. Finally, despite the myopathic changes in both sarcomere structure and function, studies revealed that the IGF-1 growth pathway was still fully functional, which provides a potential therapeutic option for patients with truncated nebulin.

Materials and Methods

Generation of the Neb$^{\Delta 163–165}$ mouse model

To create this model, the final actin-binding domain, M185, based on the previously published full murine sequence was referenced (23). Murine exon 163 contains the final three amino acids of M185 along with approximately half of the SRR. With the help of the GEMM Core at the University of Arizona, a targeting vector containing stop codons followed by a *frt-neo-frt* cassette was generated as shown in Figure 1B. The vector was transfected into 129/SvJ-derived embryonic stem cells and neomycin resistant cells were implanted into C57BL/6 J mice. Chimeras were bred with C57BL/6 J mice and *neo*-containing mice were identified via PCR using C-terminus specific primers, also shown in Figure 1B [forward (WT_F): 5′-CACACTAGAGGAATTATAGGTCAGC-3′, neo_reverse (Neo_R): 5′-CTGGCACTCTGTCGATACCC-3′]. Heterozygous mice were then bred to a separate C57BL/6 J mouse line containing a FLPase deleter to remove the neomycin cassette. Mice containing the nebulin truncation but lacking the neomycin cassette were genotyped using the same forward primer and a reverse primer to the sequence downstream from the stop codons [wt_reverse (WT_R): 5′-CCGTCACTGTATGTGGAAAGG-3′] resulting in bands as seen in Figure 1C. Mice were initially backcrossed to three generations before experiments were run and later backcrossed to generation 10 for verification purposes. All animal procedures were approved by the University of Arizona Institutional Animal Care and Use Committee.

Tissue collection

Mice were sacrificed according to approved protocols. Following the weighing of the mice, they were anesthetized via isofluorane. A toe pinch was performed to ensure complete anesthesia before cervical dislocation was performed. Hind limb muscles were then dissected and immediately flash frozen in liquid nitrogen. Following freezing, tissues were stored at −80°C. Tissue weights were normalized to tibia lengths, which were measured by electronic caliper. For each mouse, muscles from both sides were taken and weights were averaged between the two limbs. The same calculation was performed for tibia lengths before a muscle weight to tibia length normalization was performed.

Sample preparation and gel electrophoresis

Muscle samples were prepared following a well-documented protocol (42). Tissues were pulverized into a powder via glass Dounce tissue homogenizers pre-chilled in liquid nitrogen. Tissue powder was allowed to equilibrate in a −20°C refrigerator for 20 min before 50% glycerol and a urea buffer were added in a 1:40:40, sample (mg):glycerol (μL):urea (μL), ratio. Glycerol solution was made using H_2O, glycerol and a mix of inhibitors [(in mM) 0.04 E-64, 0.16 leupeptin and 0.5 PMSF]. Urea buffer contained 8 urea and 2 M thiourea, 50 tris–HCl and 75 mM

dithiothreitol, 3% SDS w/v and 0.03% bromophenol blue, with a pH of 6.8. The solution was mixed and incubated at 60°C for 10 min before being aliquoted and flash frozen in liquid nitrogen.

Myosin heavy chain gels were performed on 8% acrylamide gels as previously described, run for 24 h at 275 V before being stained with coomassie blue (43). Gels for the protein pulldown used 8% SDS-PAGE followed by staining with coomassie blue. Western blots for nebulin were run with 0.8% agarose gels run for 15 mA/gel for 2 h and 50 min before being transferred to a PVDF membrane using a semi-dry transfer unit (Bio-Rad, Hercules, CA, USA). Blots for myotilin, KLHL41 and α-actinin were run using 10% SDS-PAGE before being transferred to a PVDF membrane. All blots were initially stained with Ponceau S for protein visualization. Membranes were then blocked and incubated overnight at 4°C with the appropriate primary antibodies. Both the nebulin N-terminal antibody and the SH3 antibody were provided by Dr Siegfried Labeit (Neb-N 1:1000 rabbit, SH3 1:200 rabbit, University of Heidelberg, Mannheim, Germany). The SRR antibody was created in a chicken host against the peptide TTQLPQQR (GenScript, Piscataway, NJ, USA). Other antibodies include myotilin (1:1000 rabbit ab68915, Abcam, Cambridge, United Kingdom), KLHL41 (1:400 rabbit ab66605, Abcam), AIFM1 (1:1000 rabbit D39D2, Cell Signaling, Danvers, MA, USA) and α-actinin (1:2000 mouse A7811, Sigma-Aldrich, St. Louis, MO, USA). Western blot for nebulin domains were normalized with MHC visualized through Ponceau S. Blots run for myotilin, KLHL41 and α-actinin were normalized to GAPDH (1:2000 mouse #GA1R, Thermo Fisher, Waltham, Massachusetts, USA). Secondary antibodies used were conjugated with infrared fluorophores for detection (1:20 000 goat anti-rabbit CF680, Biotium, Fremont, CA, USA and 1:20 000 goat anti-mouse CF790, Biotium). Infrared western blot was analyzed using an Odyssey CLx Imaging System (Li-Cor Biosciences, NE, USA). MHC viewed through Ponceau S was quantified via One-D scan EX (Scanalytics Inc., Rockville, MD, USA).

Fiber type identification and CSA measurements

EDL muscles were pinned at slack length on cork and covered with OCT (Tissue-Tek). The samples were then frozen in a slurry of liquid nitrogen-cooled isopentane before being stored at −80°C. To prepare samples for cross-sections, muscles were cut mid-belly and reoriented in a cryomold containing pre-chilled OCT. Ten micron sections were collected on glass slides and stored at −20°C for no longer than 2 days (Microm HM550, Thermo Fisher). Slides were equilibrated at room temperature for 10 min while individual samples were demarcated with a hydrophobic barrier (Vector Laboratories, Burlingame, CA, USA). Then, samples were skinned using 0.2% triton X-100 for 20 min followed by a 1 h incubation with a blocking solution (2% BSA, 1% normal donkey serum) in phosphate buffered saline (PBS) at 4°C. Primary antibodies were then applied to the sections for an overnight incubation at 4°C: laminin (1:400 rabbit L9393, Sigma-Aldrich), MHCI (1:75 IgG2b BA-F8, DSHB), MHCIIA (1:500 IgG1 SC-71, DSHB), MHCIIX exclusion (1:100 IgG1 BF-35, DSHB) and MHCIIB (1:50 IgM BF-F3, DSHB). Following primary antibody incubation, sections were washed with PBS twice for 30 min. The matching secondary antibodies were then applied for 3–4 h at room temperature: polyclonal Alexa Fluor 488-conjugated goat anti-rabbit [1:500 IgG (H+L) A11008, Thermo Fisher], polyclonal Alexa Fluor 350-conjugated goat anti-mouse [1:500 IgG2b A211440, Thermo Fisher], polyclonal Alexa Fluor 350-conjugated goat anti-mouse [1:500 IgG1 A21120, Thermo Fisher] and polyclonal Alexa Fluor 594-conjugated goat anti-mouse [1:500 IgM (Heavy Chain) A21044, Thermo Fisher]. Post-secondary washes included two 30 min washes with PBS followed by two quick rinses with water. Images were collected using an AxioCam MRc (Carl Zeiss, Thornwood, NY, USA). CSAs were quantified using the semi-automatic muscle analysis using segmentation of histology (SMASH) MATLAB application (44).

RNA isolation and qRT-PCR

Tissue samples were dissected and immediately stored in RNAlater (Invitrogen, Carlsbad, CA, USA). Samples were then processed using the RNeasy Fibrous Tissue Mini Kit (Qiagen). After processing, mRNA was converted to cDNA via Superscript III (Invitrogen) and diluted to 5 ng/μL for qRT-PCR. Samples were run in triplicate using TATA-binding protein (TBP) as a house-keeping gene (TBP_qF: 5′-TGCACAGGAGCCAAGAGTGAA-3′, TBP_qR: 5′-CACATCACAGCTCCCCACCA-3′). Primers for nebulin were designed for Exon 40 (Neb_qF: 5′-CAAGGGTTACGACTTGA GACC-3′, Neb_qR: 5′-GAAAGCCAATTTGCTTGCCTC-3′). Amplification was detected using SYBR Green and run using a Rotor-Gene Q real-time PCR cycler (Qiagen). Delta–delta Ct calculations were performed with a fluorescence threshold value of 0.1.

Preparation of skinned fibers for immunofluorescence and electron microscopy

Limb muscle were dissected and immediately placed in relaxing solution (in mM: 40 BES, 10 EGTA, 6.56 $MgCl_2$, 5.88 Na-ATP, 46.35 K-proprionate and 15 creatine phosphate at pH7.0) with 1% triton X-100. At all steps, protease inhibitors were added just prior to use and samples were placed on a 2D rocker overnight at 4°C. Following skinning, muscles were washed with relaxing solution alone to remove excess triton X-100. Then, samples were placed in 50% glycerol/relaxing solution first overnight, then stored at −20°C. To obtain fiber bundles, skinned muscles were placed in sylgard dishes containing additional 50% glycerol/relaxing solution with protease inhibitors and then bundles were carefully dissected from the muscle. Bundles were held at both ends with aluminum T-clips and pinned at ∼30% past slack length.

For immunofluorescence, bundles were fixed overnight at 4°C in a 10% formalin (4% formaldehyde) solution. Post-fixation, bundles were washed with PBS before being removed from the T-clips and embedded in OCT. Longitudinal sections were taken at 6 μm and collected onto glass slides. These sections were fixed again in triton x-100 and blocked with normal donkey serum as described above. Primary antibodies to nebulin's N-terminus (1:300), M176–181 (1:100 rabbit, Siegfried Labeit), phalloidin 488 (1:2000 A12379, Invitrogen) and α-actinin were then applied for an overnight incubation at 4°C. Fluorescent secondary antibodies were applied after post-primary washes: polyclonal Alexa Fluor 594-conjugated goat anti-rabbit [1:600 IgG (H + L) A11012, Thermo Fisher] and polyclonal Alexa Fluor 350-conjugated goat anti-mouse [1:200 IgG (H + L) A21049, Thermo Fisher]. Deconvolution microscopy was performed using a Deltavision RT deconvolution microscope (Applied Precision, Issaquah, WA, USA) with an inverted microscope (IX70, Olympus, Shinjuku, Tokyo, Japan) and the softWoRx program.

For electron microscopy, fiber bundles were briefly fixed in a 3% paraformaldehyde solution [3% PF, 2% glutaraldehyde and 0.03% tannic acid in PBS (0.01 M and pH 7.2)] for 45 min at 4°C.

Then fixative was washed off with PBS and replaced with a 1% w/v OsO_4 solution in PBS. After this, fixed samples were gradually dehydrated in a series of ethanol washes, starting at 70% ethanol and ending with a mix of pure ethanol and propylene oxide. Then samples were infiltrated with resin (araldite/embed813) and then finally embedded in BEEM capsules (Ted Pella, Redding, CA, USA) for sectioning. Sections were taken at 60 µm with a diamond knife set parallel to the fiber orientation. These sections were then incubated with 1% potassium permanganate followed by 0.25% lead citrate for contrast. Images were taken with transmission electron microscopy (CM12, FEI/Philips, Hillsboro, OR, USA). Sarcomere density profiles were obtained via FIJI (ImageJ, Bethesda, MD, USA) and plot profiles were processed using the Fityk software.

Intact mechanics

Whole-muscle mechanics were done using an Aurora Scientific 1200A isolated muscle system (45,46). Briefly, the soleus or EDL were carefully extracted, keeping proximal and distal tendons intact. Silk suture loops (4–0 diameter) were tied to each tendon and the muscle was attached to both a servomotor-force transducer and a stationary hook. Muscles were submerged in an oxygenated Krebs–Ringer bicarbonate solution at 30°C (in mM: 137 NaCl, 5 KCl, 1 $NaH_2PO_4{\cdot}H_2O$, 24 $NaHCO_3$, 2 $CaCl_2{\cdot}2H_2O$, 1 $MgSO_4{\cdot}7H_2O$ and 11 glucose; pH7.5). Optimal length (L_0) was found by first performing a tetanus to remove any slack in the sutures, allowing the muscle to recover, and then increasing length until twitch forces plateaued. Force frequency relationship was determined by subjecting muscles to increasing stimulation frequencies (in Hz: 1,10, 20, 40, 60, 80, 100 and 150 for soleus with an additional 200 for EDL). Muscles were allowed to recover for 30, 30, 60, 90, 120, 120, 120 and 120 s between subsequent stimulations. Force obtained (converted to mN) was normalized to the physiological CSA (PCSA) through the following equation: PCSA = mass(mg) / [muscle density(mg/mm^3) $*$ fiber length(mm)]. The physiological density of muscle is 1.056 and fiber length was found utilizing a fiber length to muscle length ratio, 0.72 for soleus and 0.51 for EDL (47).

GST pulldown

GST fusions were made using ligation-independent cloning with vector pET His6 GST TEV LIC (2G-T), a gift from Scott Gradia (Addgene plasmid #29707). The cloned SRR and SH3 domains correspond to Uniprot Q9JL90 amino acids 629–715 and 716–768, respectively. DNA templates were prepared from C57BL/6 J soleus [RNeasy Fibrous Tissue Mini Kit (Qiagen) for RNA isolation and Superscript III (Invitrogen) for cDNA production]. Amplification of the domains used CloneAmp HiFi Polymerase (Clontech, Mountain View, CA, USA) with primers to the SRR (SRR_F: 5′-*tacttccaatccaatggagga*CGCCGGAGCCGGGACC-3′, SRR_R: 5′-*ttatccacttccaat*ACGGAAGATTTTCCCGGCAGTAGACG-3′) and the SH3 domain (SH3_F: 5′-*tacttccaatccaatggagga*GCTATATATGACTATATAGCTGCAGATGCGGATGAAGTGT-3′, SH3_R: 5′-*ttatccacttccaat*AATAGCTTCCACATAGTTGGCAGGGAGCATA-3′). Purified PCR products were cloned into SspI-linearized vector using the In-Fusion HD Cloning Kit (Clontech). The products were transformed into Stellar Competent Cells (Clontech) and spread on agar plates (100 µg/mL). Purified construct sequences were confirmed with GST_forward and T7_reverse primers recommended for the vector. To express the protein sequences, vectors were first transformed into Rosetta (DE3)pLysS Competent Cells (Novagen) and grown up in media containing ampicillin (50 µg/mL) and chloramphenicol (34 µg/mL). Protein induction was done in LB lacking chloramphenicol but containing IPTG (1 mM) at room temperature for 3–4 h. These cells were pelleted and frozen at −80°C pending further use.

To purify the protein constructs, cells were lysed in a lysis buffer [in mM: 20 Tris, 10 imidazole, 150 NaCl, 2 β-mercaptoethanol, 0.2% NP-40 and a single cOmplete protease inhibitor cocktail tablet (Sigma) per 100 mL H_2O at pH 8.0]. Lysozyme and DNaseI were added to the solution and the cells were broken apart by sonication. The mixture was centrifuged and the supernatant was filtered onto a column containing 0.5 mL Ni-NTA Agarose beads (Qiagen). Once bound, cell supernatant was washed with buffers based on the lysis buffer [5 mL of each: wash 1 (lysis without NP-40), wash 2 (wash 1 with 1 M NaCl), wash 3 (wash 1 with 25 mM imidazole)] before being eluted with 2.5 mL of an elution buffer (wash 1 with 330 mM imidazole). Fractions were analyzed via SDS-PAGE to ensure the purity of the collected GST-tagged construct (GST + SRR: 35.34 kDa, GST + SH3: 31.76 kDa and GST + SRR + SH3: 41.10 kDa).

Finally, pulldowns were performed using glutathione beads (Thermo Fisher) and whole-muscle lysate from the TC. Muscles were ground up in a glass Dounce tissue homogenizers before being incubating in a high salt lysis buffer (in mM: 100 $NaHPO_4$, 150 NaCl, 1 PMSF, 0.08 E-64, 0.376 leupeptin, 5 EGTA, 0.4% NP-40 at pH 7.5). Construct-bound glutathione beads were then incubated with the muscle lysate supernatant. After eluting the lysate solution, it was mixed with a low salt lysis buffer (0 mM $NaHPO_4$ instead of 100 mM) to make a 40 mM $NaHPO_4$ medium salt lysis solution. Beads were then incubated twice with additional medium lysis (40 mM $NaHPO_4$ from high and low lysis buffer stocks) buffer for 2.5 h each, the flow throughs being pooled together. Post-incubation, beads were washed in medium lysis buffer (5 × 10 min) before baits were denatured and released from the beads using an 8 M urea solution (in M: 8 urea, 0.05 Tris–Hcl and 0.150 NaCl at pH 8.0). To run for SDS-PAGE, eluted fractions were mixed in a 1:1 ratio with an SDS running buffer containing bromophenol blue (62.5 mM Tris–HCl at pH 6.8, 2.5% SDS, 0.002% bromophenol blue, 10% glycerol and 5% β-mercaptoethanol).

IGF-1 AAV

Viral delivery of IGF-I was used to promote muscle hypertrophy. Recombinant self-complement AAV serotype 2/8 was used to facilitate skeletal muscle targeting. The AAV harbored the cDNA sequence for murine class I *Igf-1A*, as previously described (48). This sequence includes the class I signal peptide, followed by the mature IGF-1 protein and ending with the E-peptide specific to this IGF-1 isoform. AAV serotype 2/8 was used to facilitate skeletal muscle targeting. The anterior compartment of the lower hindlimb was injected, with the TC being the target of an intramuscular injection and the EDL receiving dosages via diffusion within the compartment. Muscles were injected at 5 months of age, with one leg being treated with 2.47 × 10^{10} viral copies in 50 µL of PBS while the other leg with treated with 50 µL of PBS only. Mice were then sacrificed 1 month after injection, at 6 months of age. Following this, both TCs and EDLs were dissected and weighed. Other hind limb muscles were also weighed as negative controls. TCs were flash frozen while EDLs were pinned at slack length and embedded in OCT for cryosectioning. TCs were utilized for quantification of IGF-I content

using IGF-I ELISA (MG100, R&D Systems, Minneapolis, MN) using the manufacturer's procedures and as previously described (48).

Supplementary Material

Supplementary Material is available at *HMG* online.

Acknowledgements

Authors thanks Xiaoqun Zhou for assistance with the MHC gel work, John Smith III and Shengyi Shen for consultation on protein pull-down protocols, Justin Kolb for assistance with the IGF-1 injections and Georgios Vassilakos for performing the ELISA quantification of IGF-1 expression. Additional thanks to Siegfried Labeit for providing antibodies.

Conflict of Interest statement. None declared.

Funding

National Institute of Arthritis and Musculoskeletal and Skin Diseases of the National Institutes of Health (F31AR068849 and R01AR053897) and A Foundation Building Strength.

References

1. Pfuhl, M., Winder, S.J. and Pastore, A. (1994) Nebulin, a helical actin binding protein. *EMBO J.*, **13**, 1782–1789.
2. Labeit, S., Gibson, T., Lakey, A., Leonard, K., Zeviani, M., Knight, P., Wardale, J. and Trinick, J. (1991) Evidence that nebulin is a protein-ruler in muscle thin filaments. *FEBS Lett.*, **282**, 313–316.
3. Labeit, S. and Kolmerer, B. (1995) The complete primary structure of human nebulinand its correlation to muscle structure. *J. Mol. Biol.*, **248**, 308–315.
4. Wang, K., Knipfer, M., Huang, Q.Q., van Heerden, A., Hsu, L.C., Gutierrez, G., Quian, X.L. and Stedman, H. (1996) Human skeletal muscle nebulin sequence encodes a blueprint for thin filament architecture. Sequence motifs and affinity profiles of tandem repeats and terminal SH3. *J. Biol. Chem.*, **271**, 4304–4314.
5. Kruger, M., Wright, J. and Wang, K. (1991) Nebulin as a length regulator of thin-filaments of vertebrate skeletal-muscles—correlation of thin filament length, nebulin size, and epitope profile. *J. Cell Biol.*, **115**, 97–107.
6. Gokhin, D.S. and Fowler, V.M. (2013) A two-segment model for thin filament architecture in skeletal muscle. *Nat. Rev. Mol. Cell Biol.*, **14**, 113–119.
7. Witt, C.C., Burkart, C., Labeit, D., McNabb, M., Wu, Y., Granzier, H. and Labeit, S. (2006) Nebulin regulates thin filament length, contractility, and Z-disk structure in vivo. *EMBO J.*, **25**, 3843–3855.
8. Bang, M.L., Li, X., Littlefield, R., Bremner, S., Thor, A., Knowlton, K.U., Lieber, R.L. and Chen, J. (2006) Nebulin-deficient mice exhibit shorter thin filament lengths and reduced contractile function in skeletal muscle. *J. Cell Biol.*, **173**, 905–916.
9. Chandra, M., Mamidi, R., Ford, S., Hidalgo, C., Witt, C., Ottenheijm, C., Labeit, S. and Granzier, H. (2009) Nebulin alters cross-bridge cycling kinetics and increases thin filament activation: a novel mechanism for increasing tension and reducing tension cost. *J. Biol. Chem.*, **284**, 30889–30896.
10. Tonino, P., Pappas, C.T., Hudson, B.D., Labeit, S., Gregorio, C.C. and Granzier, H. (2010) Reduced myofibrillar connectivity and increased Z-disk width in nebulin-deficient skeletal muscle. *J. Cell Sci.*, **123**, 384–391.
11. Li, F., Buck, D., De Winter, J., Kolb, J., Meng, H., Birch, C., Slater, R., Escobar, Y.N., Smith, J.E. 3rd, Yang, L. *et al.* (2015) Nebulin deficiency in adult muscle causes sarcomere defects and muscle-type-dependent changes in trophicity: novel insights in nemaline myopathy. *Hum. Mol. Genet.*, **24**, 5219–5233.
12. Takano, K., Watanabe-Takano, H., Suetsugu, S., Kurita, S., Tsujita, K., Kimura, S., Karatsu, T., Takenawa, T. and Endo, T. (2010) Nebulin and N-WASP cooperate to cause IGF-1-induced sarcomeric actin filament formation. *Science*, **330**, 1536–1540.
13. Bang, M.L., Mudry, R.E., McElhinny, A.S., Trombitas, K., Geach, A.J., Yamasaki, R., Sorimachi, H., Granzier, H., Gregorio, C.C. and Labeit, S. (2001) Myopalladin, a novel 145-kilodalton sarcomeric protein with multiple roles in Z-disc and I-band protein assemblies. *J. Cell Biol.*, **153**, 413–427.
14. Ma, K. and Wang, K. (2002) Interaction of nebulin SH3 domain with titin PEVK and myopalladin: implications for the signaling and assembly role of titin and nebulin. *FEBS Lett.*, **532**, 273–278.
15. Eulitz, S., Sauer, F., Pelissier, M.C., Boisguerin, P., Molt, S., Schuld, J., Orfanos, Z., Kley, R.A., Volkmer, R., Wilmanns, M. *et al.* (2013) Identification of Xin-repeat proteins as novel ligands of the SH3 domains of nebulin and nebulette and analysis of their interaction during myofibril formation and remodeling. *Mol. Biol. Cell*, **24**, 3215–3226.
16. Yamamoto, D.L., Vitiello, C., Zhang, J., Gokhin, D.S., Castaldi, A., Coulis, G., Piaser, F., Filomena, M.C., Eggenhuizen, P.J., Kunderfranco, P. *et al.* (2013) The nebulin SH3 domain is dispensable for normal skeletal muscle structure but is required for effective active load bearing in mouse. *J. Cell Sci.*, **126**, 5477–5489.
17. Pelin, K., Hilpela, P., Donner, K., Sewry, C., Akkari, P.A., Wilton, S.D., Wattanasirichaigoon, D., Bang, M.L., Centner, T., Hanefeld, F. *et al.* (1999) Mutations in the nebulin gene associated with autosomal recessive nemaline myopathy. *Proc. Natl. Acad. Sci. U. S. A.*, **96**, 2305–2310.
18. Lehtokari, V.L., Pelin, K., Sandbacka, M., Ranta, S., Donner, K., Muntoni, F., Sewry, C., Angelini, C., Bushby, K., Van den Bergh, P. *et al.* (2006) Identification of 45 novel mutations in the nebulin gene associated with autosomal recessive nemaline myopathy. *Hum. Mutat.*, **27**, 946–956.
19. Lehtokari, V.L., Kiiski, K., Sandaradura, S.A., Laporte, J., Repo, P., Frey, J.A., Donner, K., Marttila, M., Saunders, C., Barth, P.G. *et al.* (2014) Mutation update: the spectra of nebulin variants and associated myopathies. *Hum. Mutat.*, **35**, 1418–1426.
20. Gurgel-Giannetti, J., Bang, M.L., Reed, U., Marie, S., Zatz, M., Labeit, S. and Vainzof, M. (2002) Lack of the C-terminal domain of nebulin in a patient with nemaline myopathy. *Muscle Nerve*, **25**, 747–752.
21. Pelin, K., Donner, K., Holmberg, M., Jungbluth, H., Muntoni, F. and Wallgren-Pettersson, C. (2002) Nebulin mutations in autosomal recessive nemaline myopathy: an update. *Neuromuscul. Disord.*, **12**, 680–686.
22. Hooper, A.C. (1978) Bone length and muscle weight in mice subjected to genetic selection for the relative length of the tibia and radius. *Life Sci.*, **22**, 283–286.
23. Kazmierski, S.T., Antin, P.B., Witt, C.C., Huebner, N., McElhinny, A.S., Labeit, S. and Gregorio, C.C. (2003)

The complete mouse nebulin gene sequence and the identification of cardiac nebulin. *J. Mol. Biol.*, **328**, 835–846.
24. Ottenheijm, C.A., Buck, D., de Winter, J.M., Ferrara, C., Piroddi, N., Tesi, C., Jasper, J.R., Malik, F.I., Meng, H., Stienen, G.J. *et al.* (2013) Deleting exon 55 from the nebulin gene induces severe muscle weakness in a mouse model for nemaline myopathy. *Brain*, **136**, 1718–1731.
25. North, K.N., Laing, N.G. and Wallgren-Pettersson, C. (1997) Nemaline myopathy: current concepts. The ENMC International Consortium and Nemaline Myopathy. *J. Med. Genet.*, **34**, 705–713.
26. Luther, P.K. (2009) The vertebrate muscle Z-disc: sarcomere anchor for structure and signalling. *J. Muscle Res. Cell Motil.*, **30**, 171–185.
27. Selcen, D. and Engel, A.G. (2004) Mutations in myotilin cause myofibrillar myopathy. *Neurology*, **62**, 1363–1371.
28. Gupta, V.A., Ravenscroft, G., Shaheen, R., Todd, E.J., Swanson, L.C., Shiina, M., Ogata, K., Hsu, C., Clarke, N.F., Darras, B.T. *et al.* (2013) Identification of KLHL41 mutations implicates BTB-Kelch-mediated ubiquitination as an alternate pathway to myofibrillar disruption in nemaline myopathy. *Am. J. Hum. Genet.*, **93**, 1108–1117.
29. Ghezzi, D., Sevrioukova, I., Invernizzi, F., Lamperti, C., Mora, M., D'Adamo, P., Novara, F., Zuffardi, O., Uziel, G. and Zeviani, M. (2010) Severe X-linked mitochondrial encephalomyopathy associated with a mutation in apoptosis-inducing factor. *Am. J. Hum. Genet.*, **86**, 639–649.
30. Ogilvie, I., Pourfarzam, M., Jackson, S., Stockdale, C., Bartlett, K. and Turnbull, D.M. (1994) Very long-chain acyl coenzyme A dehydrogenase deficiency presenting with exercise-induced myoglobinuria. *Neurology*, **44**, 467–467.
31. Peralta, S., Goffart, S., Williams, S.L., Diaz, F., Garcia, S., Nissanka, N., Area-Gomez, E., Pohjoismaki, J. and Moraes, C.T. (2018) ATAD3 controls mitochondrial cristae structure in mouse muscle, influencing mtDNA replication and cholesterol levels. *J. Cell Sci.*, **131**.
32. Salmikangas, P., Mykkänen, O.-M., Grönholm, M., Heiska, L., Kere, J. and Carpén, O. (1999) Myotilin, a novel sarcomeric protein with two Ig-like domains, is encoded by a candidate gene for limb-girdle muscular dystrophy. *Hum. Mol. Genet.*, **8**, 1329–1336.
33. Lee, E.J., De Winter, J.M., Buck, D., Jasper, J.R., Malik, F.I., Labeit, S., Ottenheijm, C.A. and Granzier, H. (2013) Fast skeletal muscle troponin activation increases force of mouse fast skeletal muscle and ameliorates weakness due to nebulin-deficiency. *PLoS One*, **8**, e55861.
34. de Winter, J.M., Buck, D., Hidalgo, C., Jasper, J.R., Malik, F.I., Clarke, N.F., Stienen, G.J., Lawlor, M.W., Beggs, A.H., Ottenheijm, C.A. *et al.* (2013) Troponin activator augments muscle force in nemaline myopathy patients with nebulin mutations. *J. Med. Genet.*, **50**, 383–392.
35. Zierath, J.R. and Hawley, J.A. (2004) Skeletal muscle fiber type: influence on contractile and metabolic properties. *PLoS Biol.*, **2**, e348.
36. Liu, J., Liang, X. and Gan, Z. (2015) Transcriptional regulatory circuits controlling muscle fiber type switching. *Sci. China Life Sci.*, **58**, 321–327.
37. Panaviene, Z. and Moncman, C.L. (2007) Linker region of nebulin family members plays an important role in targeting these molecules to cellular structures. *Cell Tissue Res.*, **327**, 353–369.
38. van der Ven, P.F., Wiesner, S., Salmikangas, P., Auerbach, D., Himmel, M., Kempa, S., Hayess, K., Pacholsky, D., Taivainen, A., Schroder, R. *et al.* (2000) Indications for a novel muscular dystrophy pathway. gamma-filamin, the muscle-specific filamin isoform, interacts with myotilin. *J. Cell Biol.*, **151**, 235–248.
39. Hangen, E., Blomgren, K., Benit, P., Kroemer, G. and Modjtahedi, N. (2010) Life with or without AIF. *Trends Biochem. Sci.*, **35**, 278–287.
40. Garvey, S.M., Liu, Y., Miller, S.E. and Hauser, M.A. (2008) Myotilin overexpression enhances myopathology in the LGMD1A mouse model. *Muscle Nerve*, **37**, 663–667.
41. Ramirez-Martinez, A., Cenik, B.K., Bezprozvannaya, S., Chen, B., Bassel-Duby, R., Liu, N. and Olson, E.N. (2017) KLHL41 stabilizes skeletal muscle sarcomeres by nonproteolytic ubiquitination. *Elife*, **6**, e26439.
42. Warren, C.M., Krzesinski, P.R. and Greaser, M.L. (2003) Vertical agarose gel electrophoresis and electroblotting of high-molecular-weight proteins. *Electrophoresis*, **24**, 1695–1702.
43. Talmadge, R.J. and Roy, R.R. (1993) Electrophoretic separation of rat skeletal muscle myosin heavy-chain isoforms. *J. Appl. Physiol.*, **75**, 2337–2340.
44. Smith, L.R. and Barton, E.R. (2014) SMASH—semi-automatic muscle analysis using segmentation of histology: a MATLAB application. *Skelet. Muscle*, **4**, 21.
45. Labeit, S., Kohl, C.H., Witt, C.C., Labeit, D., Jung, J. and Granzier, H. (2010) Modulation of muscle atrophy, fatigue and MLC phosphorylation by MuRF1 as indicated by hindlimb suspension studies on MuRF1-KO mice. *J. Biomed. Biotechnol.*, **2010**, 693741.
46. Ottenheijm, C.A., Hidalgo, C., Rost, K., Gotthardt, M. and Granzier, H. (2009) Altered contractility of skeletal muscle in mice deficient in titin's M-band region. *J. Mol. Biol.*, **393**, 10–26.
47. Burkholder, T.J., Fingado, B., Baron, S. and Lieber, R.L. (1994) Relationship between muscle fiber types and sizes and muscle architectural properties in the mouse hindlimb. *J. Morphol.*, **221**, 177–190.
48. Barton, E.R. (2006) Viral expression of insulin-like growth factor-I isoforms promotes different responses in skeletal muscle. *J. Appl. Physiol.*, **100**, 1778–1784.